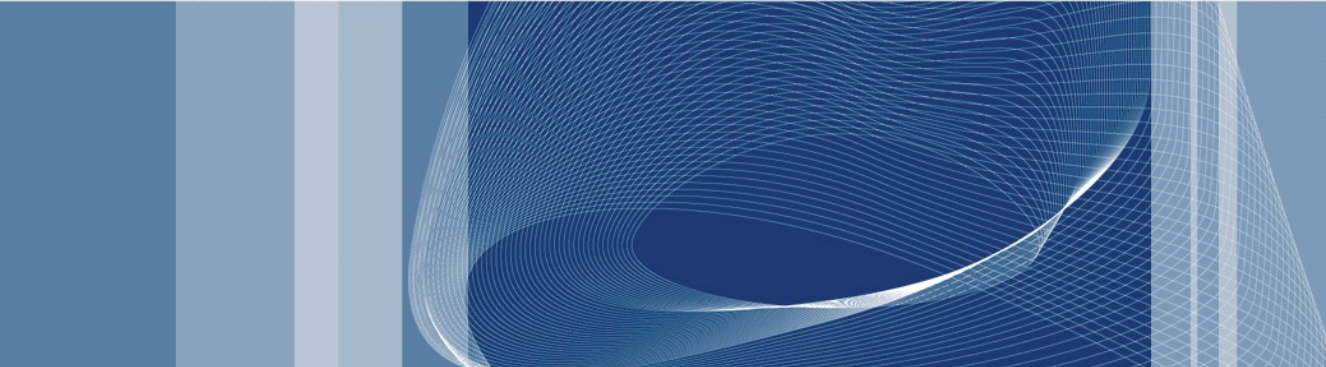


POLITECNICO DI MILANO



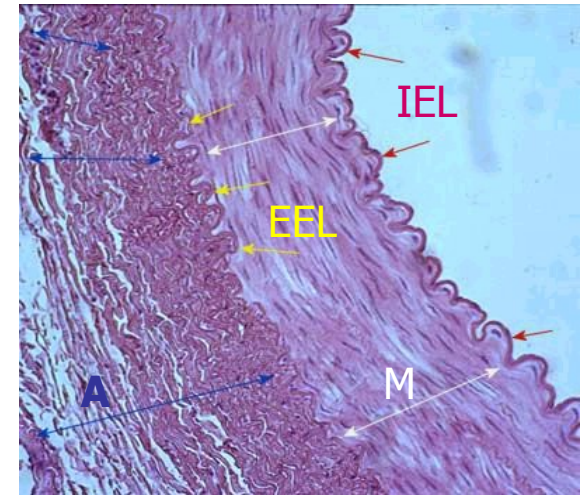
A Numerical Model of Atherosclerotic Lesions in Human Arteries

Anna Ferrara

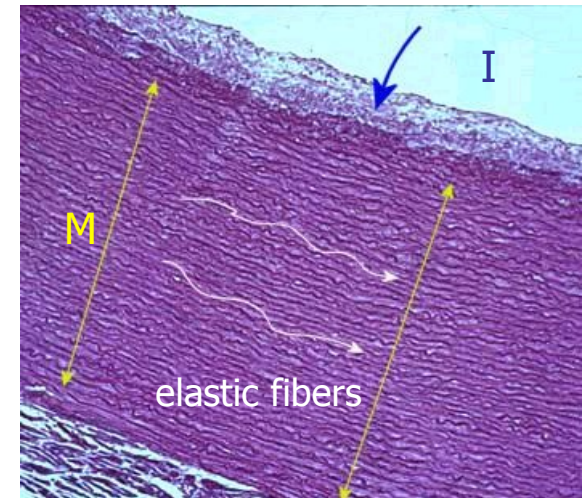
Università degli Studi di Pavia – Dipartimento di Meccanica Strutturale

Pavia, 19 ottobre 2009

- At microscopic level the arterial wall shows a layered structure, made of three concentric zones:
 - tunica adventitia (A);
 - tunica media (M);
 - tunica intima (I);separated by elastic laminae (IEL, EEL).
- Each layer wall is a composite structure containing, in different proportions:
 - elastin;
 - collagen;
 - endothelial and smooth muscle cells,
 - and ground matrix.
- Arteries can be subdivided into:
 - muscular artery and elastic artery.



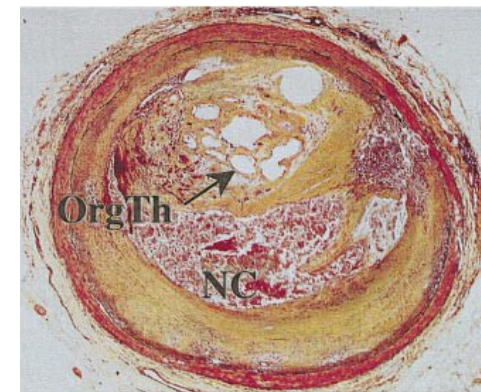
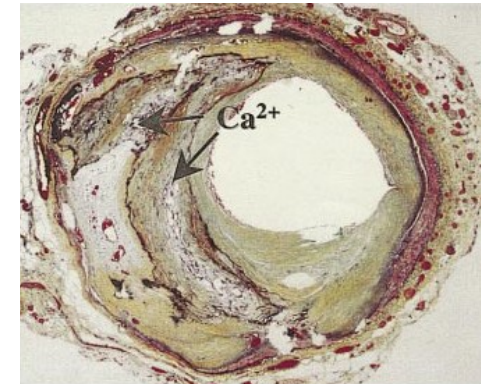
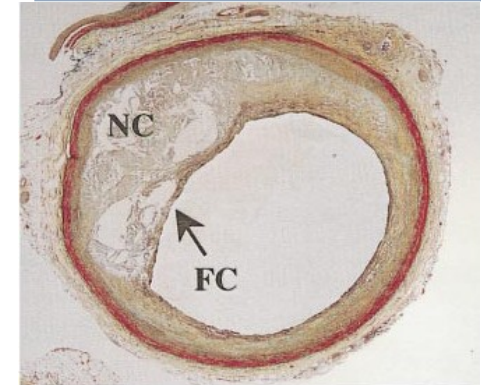
Muscular artery (coronaries)



Elastic artery (aorta)

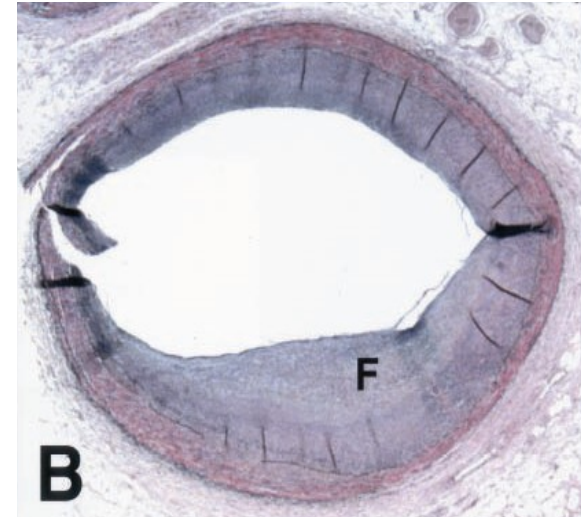
Atherosclerosis

- **Atherosclerosis** is a vascular disease characterized by [Virmani et al., 2000]:
 - infiltration of lipids, inflammatory cells into the intima and formation of the **plaque**;
 - narrowing of the arterial lumen (**stenosis**), and obstruction of the blood flow.
- The **plaque core**, separated from the lumen by a **fibrous cap** (collagen and smooth muscle cell), may contain:
 - a **lipid pool** (foam cells and debris);
 - **calcification**.
- Angiographic studies proved positive correlations between **spontaneous plaque rupture** and:
 - myocardial infarction;
 - unstable angina;
 - thrombus formation (**atherothrombosis**).

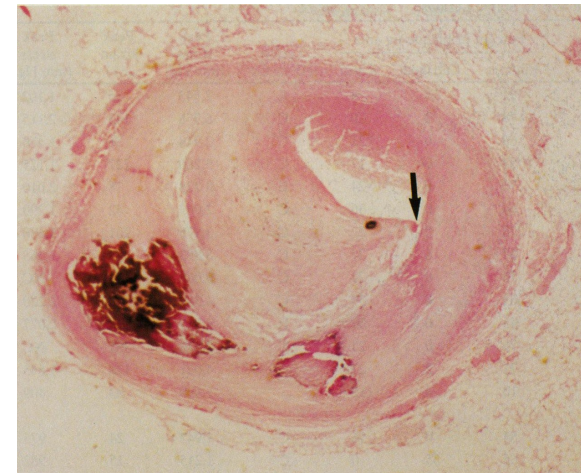


Plaque Rupture

- The risk of plaque rupture [*Pasterkamp et al., 2000*] is related to :
 - the vulnerability of individual plaques (intrinsic disease);
 - rupture triggers (extrinsic dynamic forces).
- **Vulnerable plaque**, characterized by:
 - non calcified, eccentric plaque;
 - a thin fibrous cap ($< 65 \mu\text{m}$);
 - a large lipid pool ($> 40\%$ plaque area),are prone to rupture.
- Plaque rupture manifests at the shoulder as provided in 64% of cases in an autopsy series [*Richardson et al., 1989*].



[*Yabushita et al., 2002*]



[*Cheng et al., 1993*]

GOAL: want to setup a realistic numerical tool able to simulate fracture in human arteries such as:

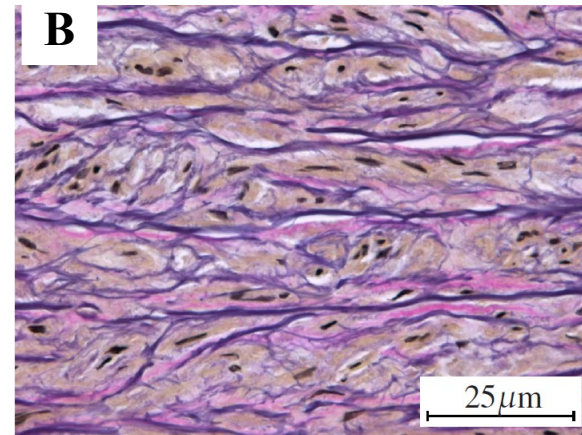
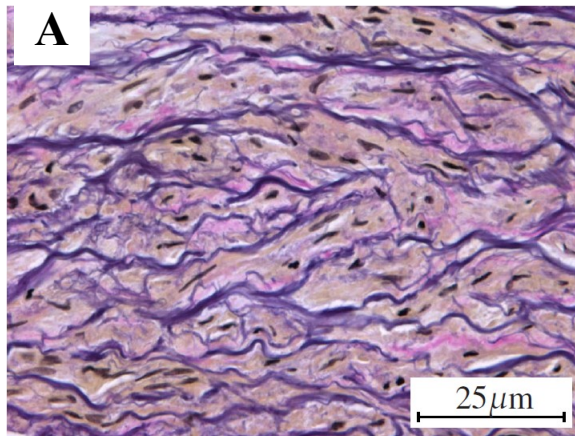
- plaque rupture;
- spontaneous dissection between artery layers.

■ Need to use:

- **Geometrical model** of healthy/diseased arteries, obtained through magnetic resonance or ultrasound imaging.
- **Material model**, built up by considering the underlying micro-structural composition of the tissue: two sets of reinforcing collagen fibers.
- **Damage/deterioration/fracture** model able to describe the breaking of the plaque and the dissection of a layer.

- In each arterial layers, the isotropic ground matrix is reinforced by two families of collagen fibers [*Patel et al., 1969*].
- Histological evidence [*Shekhonin et al. 1985*] proves:
 - large dispersion of collagen fibers in the intima and adventitia;
 - alignment of the collagen fibers along the circumferential direction with a very little dispersion in the media.

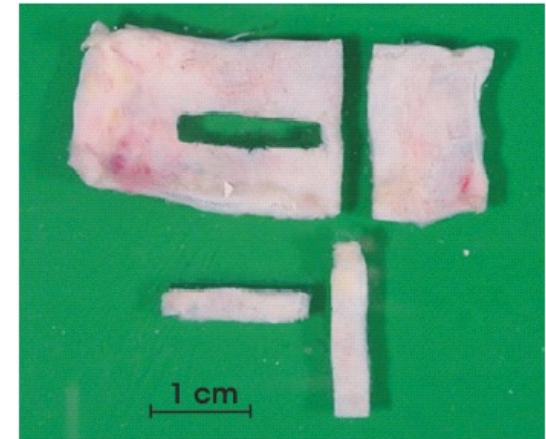
Aortic media (a) unstretched (b) stretched



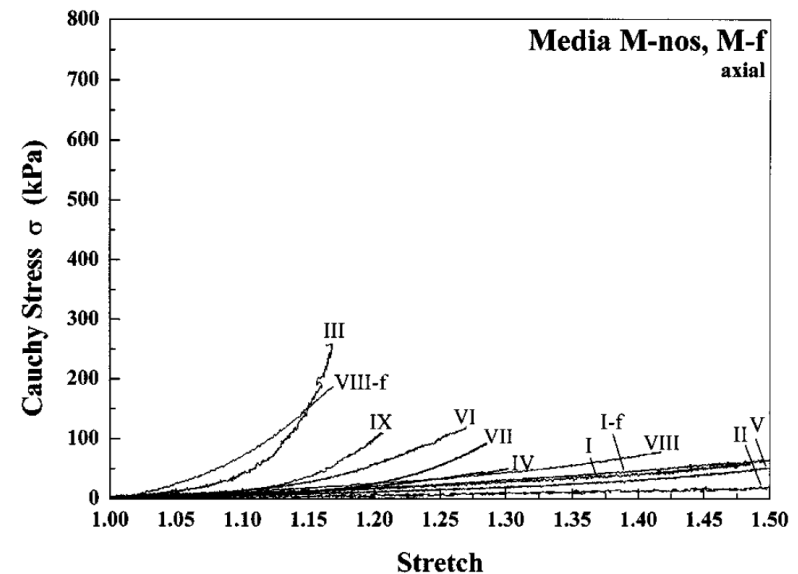
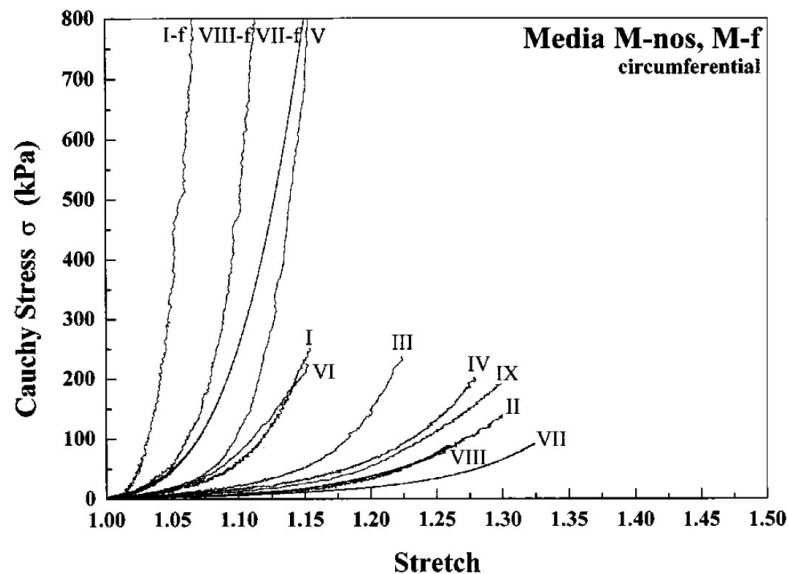
[*Sommer et al., 2008*]

Anisotropy in Uniaxial Tests

- Uniaxial tension tests of human iliac strips (axial and circumferential samples) provide stiffness and resistance data [Holzapfel et al. 2004].
- Experiments show a different response of the material in the circumferential and in the axial direction:
 - media is stiffer in circumferential (left) than in axial (right) direction.



[Holzapfel et al., 2004]



- An elastic material is called **hyperelastic** when its constitutive law derives from a strain energy function Ψ (Helmoltz free energy).
For **anisotropic elastic material**, the strain energy function Ψ may be expressed in terms of the Cauchy-Green tensor \mathbf{C} and of the two structural tensors \mathbf{A}_0 and \mathbf{G}_0 [*Spencer, 1984*]:

$$\Psi = \Psi (\mathbf{C}, \mathbf{A}_0, \mathbf{G}_0), \quad \mathbf{A}_0 = \mathbf{a}_0 \otimes \mathbf{a}_0, \quad \mathbf{G}_0 = \mathbf{g}_0 \otimes \mathbf{g}_0.$$

- **Material frame indifference** is satisfied if the strain energy function respects the condition:

$$\Psi (\mathbf{C}, \mathbf{A}_0, \mathbf{G}_0) = \Psi (\mathbf{Q}\mathbf{C}\mathbf{Q}^T, \mathbf{Q}\mathbf{A}_0\mathbf{Q}^T, \mathbf{Q}\mathbf{G}_0\mathbf{Q}^T), \quad \mathbf{Q} \in \text{SO}(3).$$

- According to [*Spencer, 1984*], the above condition implies that the strain energy function Ψ is a function of the three **isotropic invariants** of \mathbf{C} and of the six pseudo invariants (**anisotropic invariants**):

$$\Psi (\mathbf{C}, \mathbf{A}_0, \mathbf{G}_0) = \Psi (J, I_1, I_2, I_3, I_4, I_5, I_6, I_7, I_8, I_9).$$

- Assumption: **incompressible materials** are modeled as slightly compressible materials.
Decoupled near-incompressible elasticity: the strain energy decomposes into the sum of a **volumetric**, an **isotropic** and an **anisotropic** parts, each depending on a few single parameters:

$$\Psi = \Psi_{\text{vol}}(J) + \Psi_{\text{iso}}(\bar{I}_1, \bar{I}_2) + \Psi_{\text{aniso}}(\bar{I}_4, \bar{I}_6).$$

- According to *[Patel et al., 1969]* the two families of collagen fibers are equivalent in stiffness and strength.
The uniaxial response of each fiber family is given by an exponential function (that excludes compressive behaviors) *[Holzapfel et al. 2000]*.
- The single terms of the strain energy function Ψ are:

$$\Psi_{\text{vol}}(J) = \frac{K}{2} \log J, \quad \Psi_{\text{iso}}(\bar{I}_1) = \frac{\mu_1}{2} (\bar{I}_1 - 3),$$
$$\Psi_{\text{aniso}}(\bar{I}_4, \bar{I}_6) = \frac{k_1}{2k_2} \sum_{i=4,6} \left(\exp \left[k_2 (\bar{I}_i - 1)^2 \right] - 1 \right).$$

- Decouple the volumetric and the isochoric deformation:

$$J = \det \mathbf{F}, \quad \bar{\mathbf{F}} = (J^{-1/3} \mathbf{I}) \mathbf{F}, \quad \bar{\mathbf{C}} = \bar{\mathbf{F}}^T \bar{\mathbf{F}} = J^{-2/3} \mathbf{C}.$$

- Three isotropic invariants of the modified Cauchy-Green tensor:

$$\bar{I}_1 = \text{tr}(\bar{\mathbf{C}}), \quad \bar{I}_2 = \frac{1}{2} \left[I_1^2 - \text{tr}(\bar{\mathbf{C}}^2) \right], \quad \bar{I}_3 = \det(\bar{\mathbf{C}}) = 1.$$

- Two most significant pseudo-invariants of the modified Cauchy-Green tensor and of the structural tensors \mathbf{A}_0 , \mathbf{G}_0 (square of the stretch of the material in the fiber direction):

$$\bar{I}_4 = \lambda_a^2 = \mathbf{a} \cdot \mathbf{a} = \mathbf{a}_0 \cdot \bar{\mathbf{C}} \mathbf{a}_0, \quad \bar{I}_6 = \lambda_g^2 = \mathbf{g} \cdot \mathbf{g} = \mathbf{g}_0 \cdot \bar{\mathbf{C}} \mathbf{g}_0.$$

- Higher order invariants [*Merodio et al., 2003; 2005*]:

$$\begin{aligned} \bar{I}_5 &= \mathbf{a}_0 \cdot (\bar{\mathbf{C}}^2 \mathbf{a}_0), & \bar{I}_7 &= \mathbf{g}_0 \cdot (\bar{\mathbf{C}}^2 \mathbf{g}_0); \\ \bar{I}_8 &= \mathbf{a}_0 \cdot (\bar{\mathbf{C}} \mathbf{g}_0), & \bar{I}_9 &= (\mathbf{a}_0 \cdot \mathbf{g}_0)^2. \end{aligned}$$

- Given an hyperelastic materials the stress are given by differentiation with respect to the strain measures: *[Holzapfel et al. 2000]*

$$\mathbf{S} = 2 \frac{\partial \Psi (\mathbf{C}, \mathbf{A}_0, \mathbf{G}_0)}{\partial \mathbf{C}}, \quad \mathbf{S} = \mathbf{S}_{\text{vol}} + \mathbf{S}_{\text{iso}} + \mathbf{S}_{\text{aniso}}.$$

$$\mathbf{S} = p J \mathbf{C}^{-1} + J^{-2/3} \mathbb{P} : 2 \left[\frac{\partial \Psi_{\text{iso}} (\bar{\mathbf{C}})}{\partial \bar{\mathbf{C}}} + \frac{\partial \Psi_{\text{aniso}} (\bar{\mathbf{C}})}{\bar{\mathbf{C}}} \right].$$

where:

$$p = \frac{d\Psi_{\text{vol}}(J)}{dJ}, \quad \mathbb{P} = \mathbb{I} - \frac{1}{3} \mathbf{C}^{-1} \otimes \mathbf{C}.$$

- Stress tensor for the arterial layers:

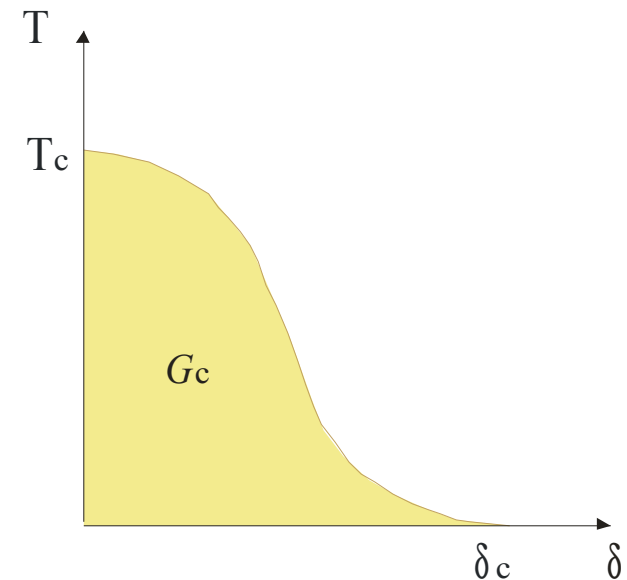
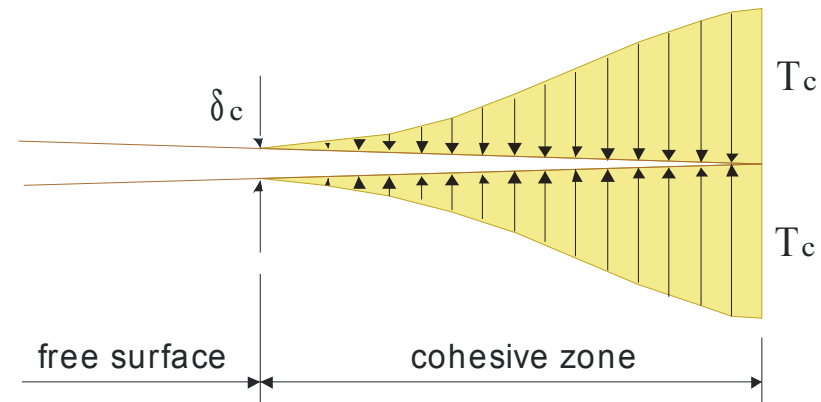
$$\mathbf{S} = \frac{K}{2} \mathbf{C}^{-1} + J^{-2/3} \mathbb{P} : 2 \left[\frac{\mu_1}{2} \mathbf{I} + k_1 (\bar{I}_4 - 1) \exp \left[k_2 (\bar{I}_4 - 1)^2 \right] \mathbf{A}_0 \right. \\ \left. + k_1 (\bar{I}_6 - 1) \exp \left[k_2 (\bar{I}_6 - 1)^2 \right] \mathbf{G}_0 \right]$$

Interface Models

- Rupture may be explicitly simulated by the adaptive insertion of fracture surfaces (alternative to damage models).
- Cohesive models (originally developed for isotropic materials):
 - existence of a cohesive zone ahead of the crack tip;
 - the progressive opening of the fracture (opening displacement) δ is resisted by cohesive traction \mathbf{T} acting on the cohesive zone;
 - tractions are related to the displacement jump by a cohesive law $\mathbf{T}(\delta)$.

[Dugdale, 1960; Barenblatt, 1962]

[Needleman, 1992; Camacho and Ortiz, 1996]



- The mixed-mode isotropic model proposed in [*Ortiz and Pandolfi, 1999*] extended to anisotropy by introducing a dependence of the material properties on the direction.
- Anisotropy reflects in:
 - **insertion criterion** (when and where a fracture surface must be inserted);
 - **cohesive behavior** (how the cohesive surface behaves).
- The **cohesive free energy density** Φ must distinguish between opening (mode I) and sliding (mode II and mode III) behavior. Assume:
 - Isothermal process;
 - cohesive response independent of stretching and shearing of the cohesive surface (depends only on the displacement jump);
 - explicit dependence on the deformed local main anisotropy directions and on some internal variable \mathbf{q} (maximum displacement jump):

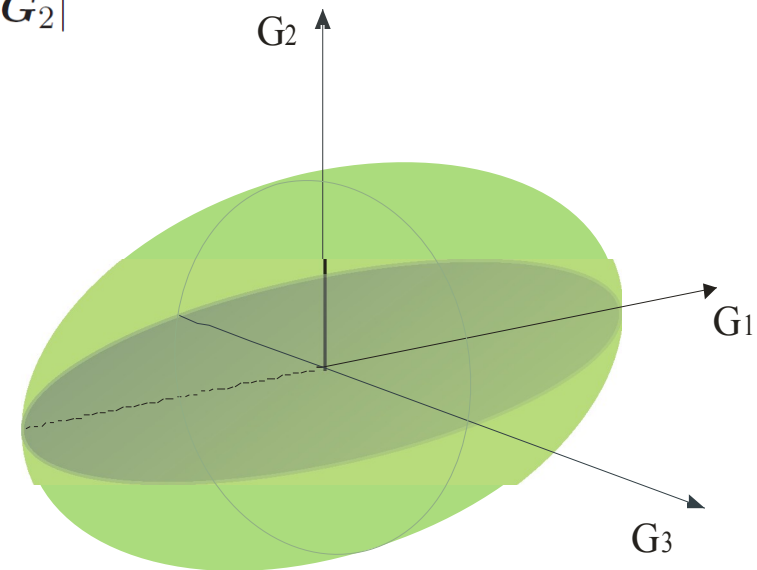
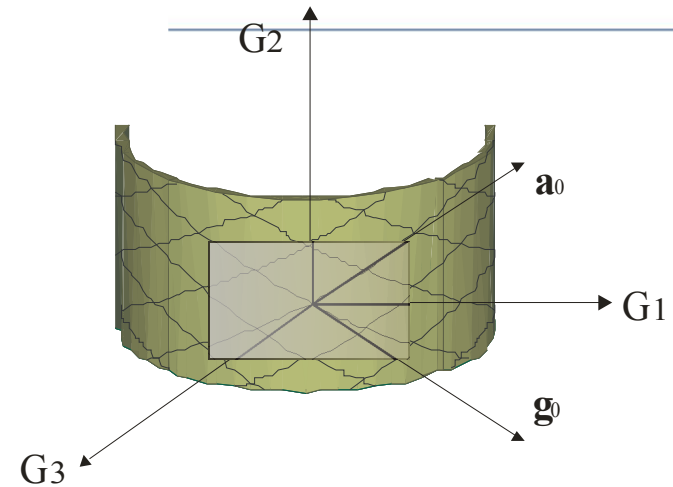
$$\Phi = \Phi (\delta^1, \delta^2, \delta^3, \mathbf{q}) .$$

Anisotropic Resistance Surface

- Two equivalent families of fibers oriented along \mathbf{a}_0 and \mathbf{g}_0 identify three principal anisotropy directions \mathbf{G}_1 , \mathbf{G}_2 , \mathbf{G}_3 in the reference space:
 - \mathbf{G}_1 , \mathbf{G}_2 (bisectors of the angles formed by the fibers); \mathbf{G}_3 (normal to their plane).

$$\mathbf{G}_1 = \frac{\mathbf{a}_0 + \mathbf{g}_0}{|\mathbf{a}_0 + \mathbf{g}_0|}, \quad \mathbf{G}_2 = \frac{\mathbf{a}_0 - \mathbf{g}_0}{|\mathbf{a}_0 - \mathbf{g}_0|}, \quad \mathbf{G}_3 = \frac{\mathbf{G}_1 \times \mathbf{G}_2}{|\mathbf{G}_1 \times \mathbf{G}_2|}.$$

- The resistance changes with the spatial orientation in the form of ellipsoidal surface [Yu et al. 2002]:
 - different tensile resistance are associated to each principal directions $\sigma_{c1} \geq \sigma_{c2} \geq \sigma_{c3}$;
 - cohesive energies change proportionally $\mathbf{G}_{c1} \geq \mathbf{G}_{c2} \geq \mathbf{G}_{c3}$.



- Given a potential fracture plane and the normal axis along the direction \mathbf{N} , compute the intersections of axis and plane with the resistance ellipsoid.
- The axis provides the normal opening values of the local normal cohesive resistance $\sigma_3(\mathbf{N}) = \sigma_c(\mathbf{N})$ and of the local normal fracture energy $G_{3L} = G_c(\mathbf{N})$;
- The plane provides an ellipsis, whose principal axes define the local principal cohesive sliding directions \mathbf{M}_{1L} , and \mathbf{M}_{2L} ; the resistances, σ_{1L} , σ_{2L} ; and the fracture energies G_{1L} , G_{2L} for the plane itself.
- Under change of configuration due to motion, the three principal axes of anisotropy \mathbf{m}_1 , \mathbf{m}_2 , $\mathbf{m}_3 = \mathbf{n}$ are calculated by the deformation gradient \mathbf{F}_s of the cohesive surface :

$$\mathbf{m}_1 = \frac{\mathbf{F}_S \mathbf{M}_1}{|\mathbf{F}_S \mathbf{M}_1|}, \quad \mathbf{m}_2 = \frac{\mathbf{F}_S \mathbf{M}_2}{|\mathbf{F}_S \mathbf{M}_2|}, \quad \mathbf{m}_3 = \frac{\mathbf{m}_1 \times \mathbf{m}_2}{|\mathbf{m}_1 \times \mathbf{m}_2|},$$

Anisotropic Cohesive Law

- Once a free energy density has been defined, the cohesive law follows as:

$$\mathbf{T} = \frac{\partial \Phi}{\partial \boldsymbol{\delta}} (\delta^1, \delta^2, \delta^3, \mathbf{q}).$$

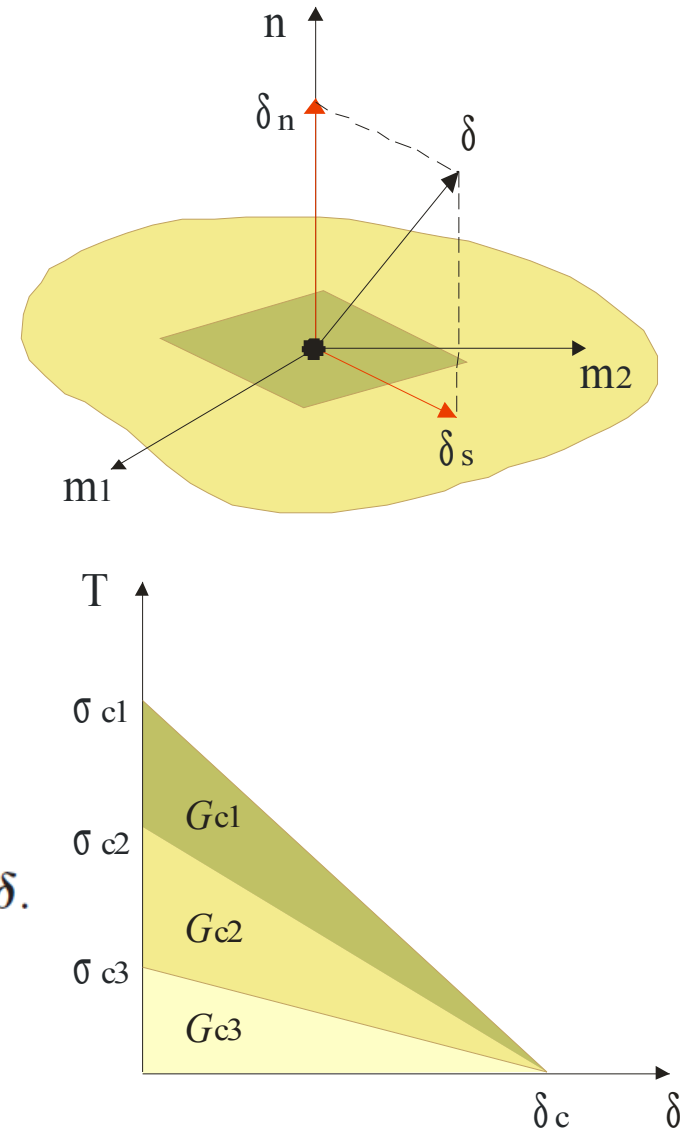
- Following [Camacho and Ortiz. 1999], introduce effective measure of opening displacement and tractions:

$$\delta = \sqrt{\beta^2 [(\delta^1)^2 + \alpha^2 (\delta^2)^2] + (\delta^n)^2}.$$

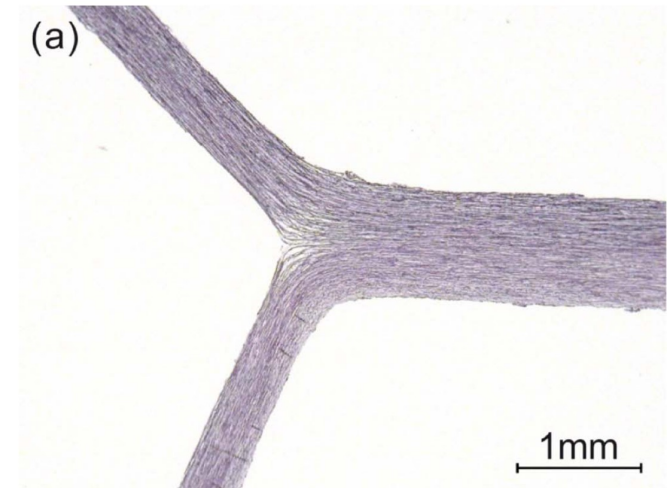
the cohesive law takes the form:

$$\mathbf{T} = \frac{T}{\delta} [\beta^2 (\mathbf{m}_1 \otimes \mathbf{m}_1 + \alpha^2 \mathbf{m}_2 \otimes \mathbf{m}_2) + \mathbf{n} \otimes \mathbf{n}] \boldsymbol{\delta}.$$

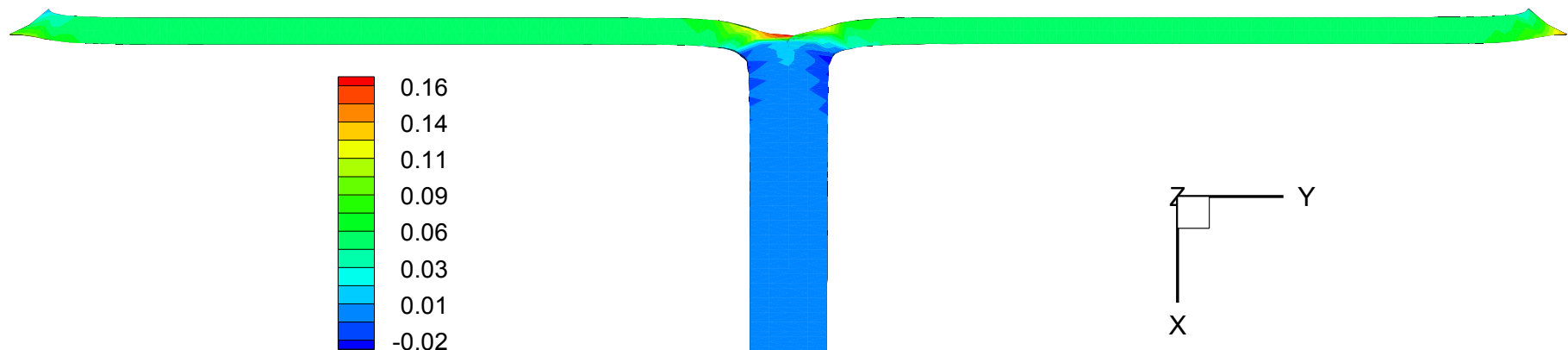
- Use a linearly decreasing loading envelope.



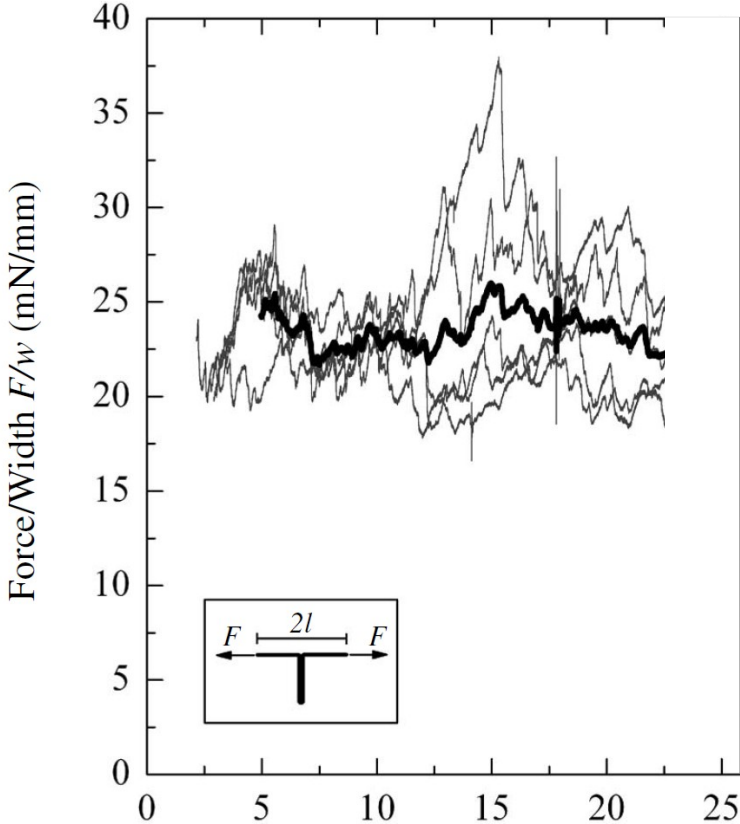
- Aortic media during peeling in circumferential directions [*Sommer et al. 2008*].
- FE analysis performed by assuming a full anisotropy, induced by fibers, of the bulk and of the cohesive surface [*Ferrara and Pandolfi, 2009*].
- Deformed configuration of the aorta specimen after application of the whole displacement.



[*Sommer et al., 2008*]

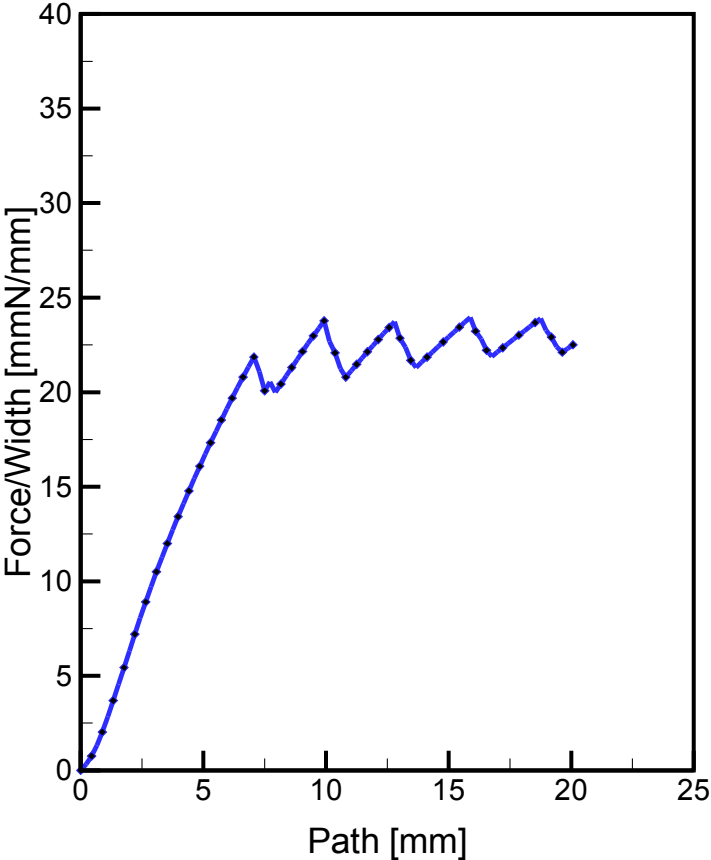


Peeling test in circumferential direction



[Sommer et al., 2008]

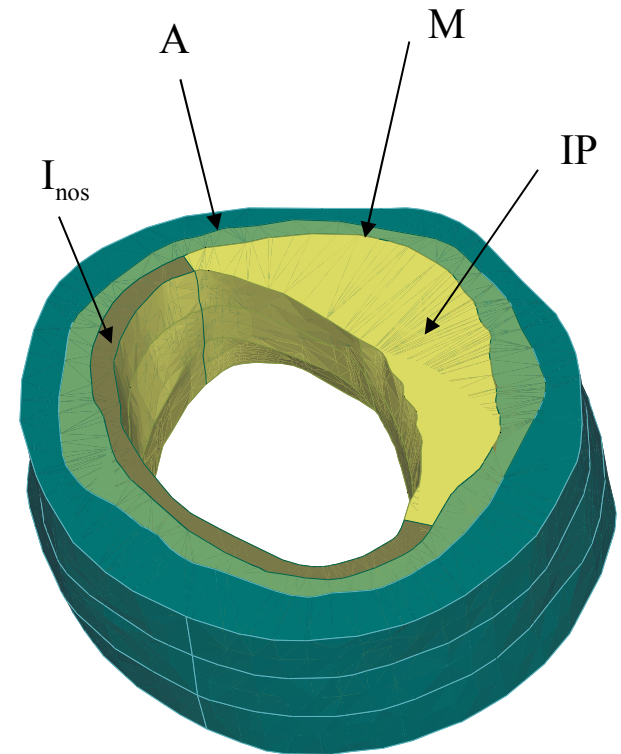
Numerical test results



[Ferrara and Pandolfi., 2009]

Geometry of Human Arteries

- Reconstructed by manual segmentation of high-resolution magnetic resonance images (MRI) of a human iliac artery [Yang et al., 2003].
- Four digitized cross-sections at 1.5mm distance showing healthy and diseased tissues are identified clearly.
- The model is characterized by an eccentric plaque of fibrous connective tissue, and a stenosis of about 40%.
- Lipid pool is a fluid with gel consistence not able to sustain shear stresses, [Loree et al., 1994]; [Richardson et al., 1989].

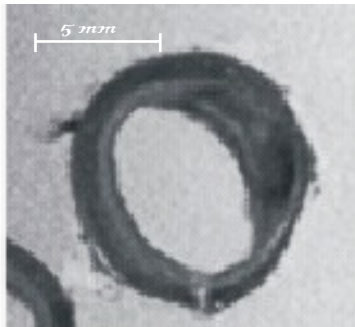
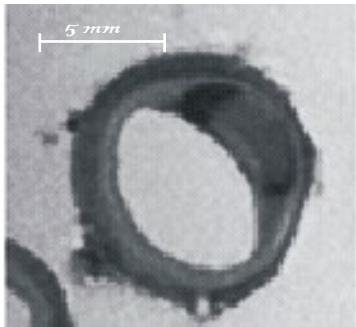
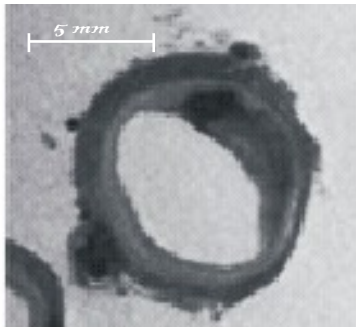
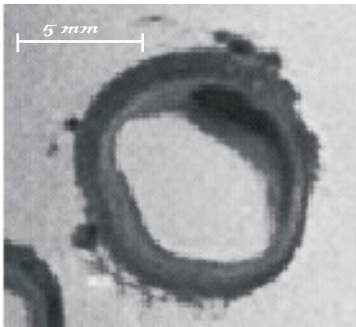


slice # 1

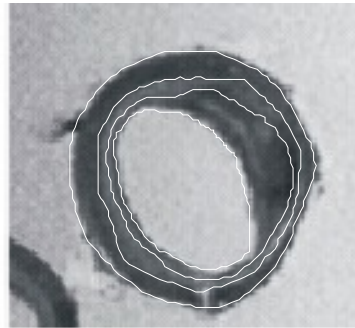
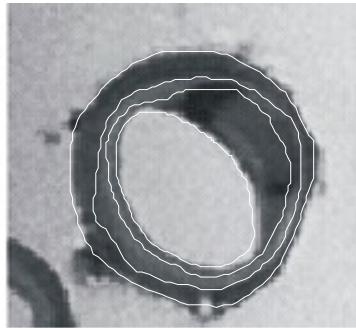
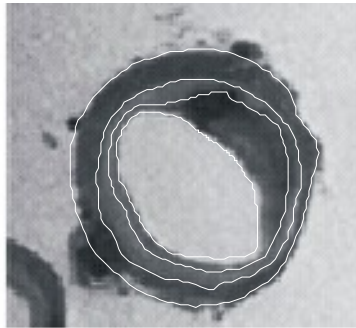
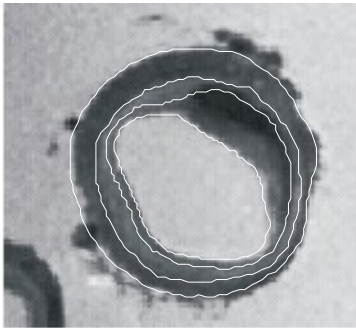
slice # 2

slice # 3

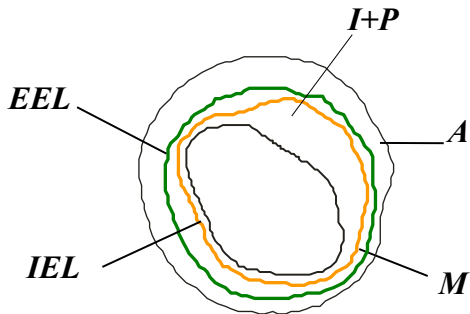
slice # 4



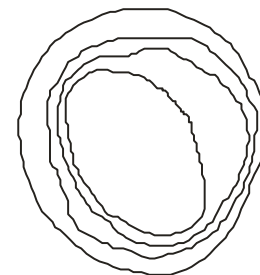
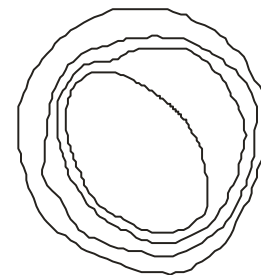
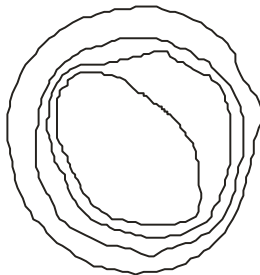
MR images
0.3 mm/pixel
1.2 mm



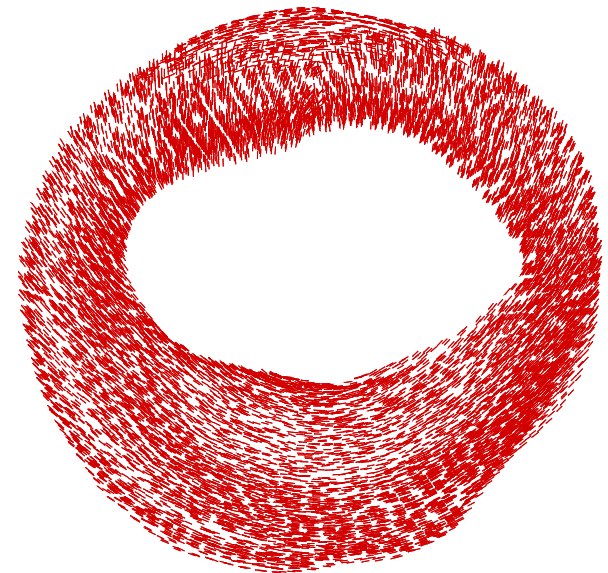
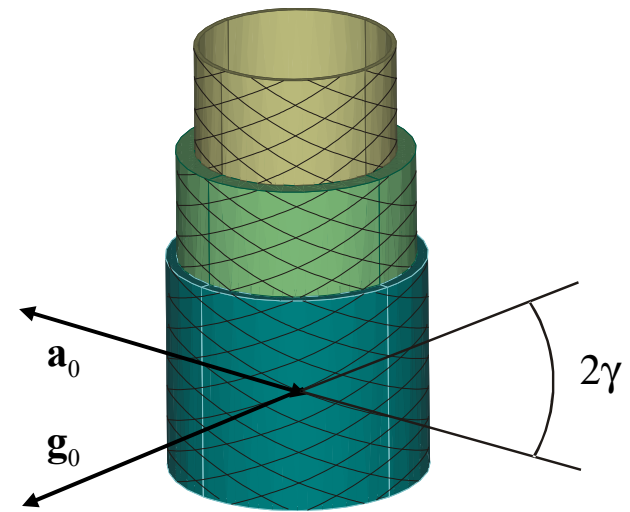
digitized
contours

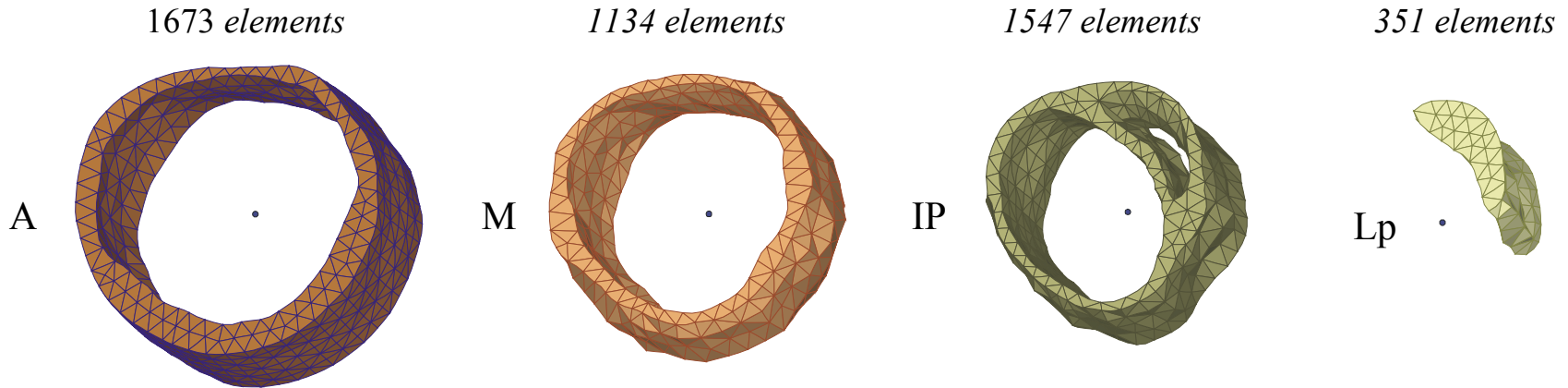


region
borders

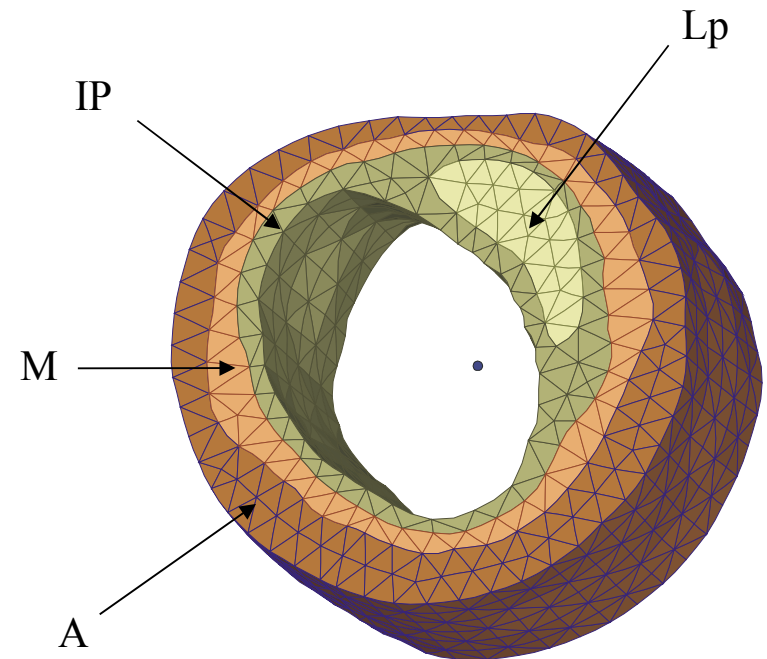


- Idealization [Holzapfel et al., 2000, 2004] fibers are inclined in two directions \mathbf{a}_0 and \mathbf{g}_0 with respect to the circumferential direction, forming a constant angle 2γ different for each layer:
 - $\gamma = 49^\circ$ adventitia;
 - $\gamma = 7^\circ$ media;
 - $\gamma = 5^\circ$ healthy intima;
 - $\gamma = 0^\circ$ diseased intima.
- The two set of fibers are equivalent, and their geometrical organization defines an *orthotropic structure*.
- Top view of the fiber distribution in the arterial model.





- Layered (intima, media, adventitia) model of a damaged human artery (7437 nodes and 4201 tetrahedra).
- Anisotropic two-fibers material model [Holzapfel et al., 2004].
- Acoustic material for lipid pool [Mota et al., 2007].
- Anisotropic cohesive law [Ferrara e Pandolfi, 2008].

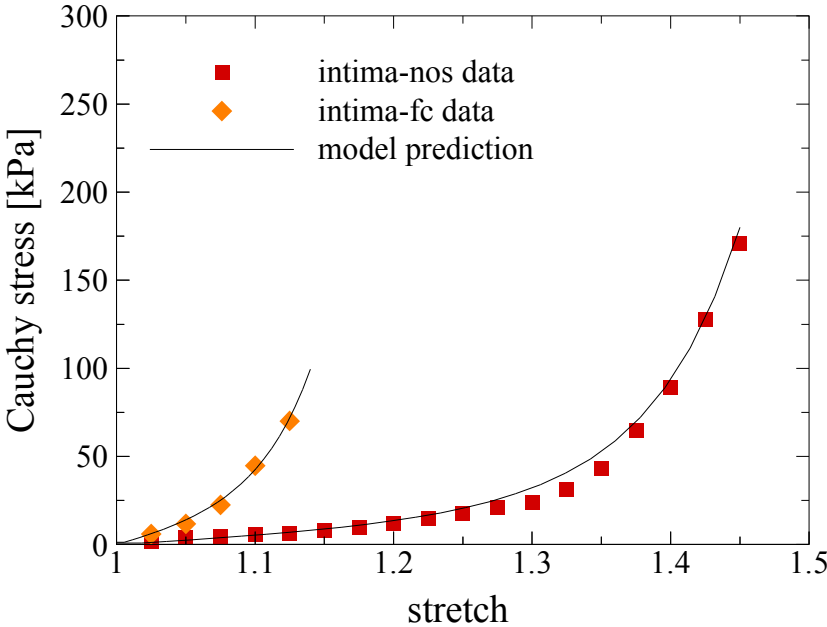
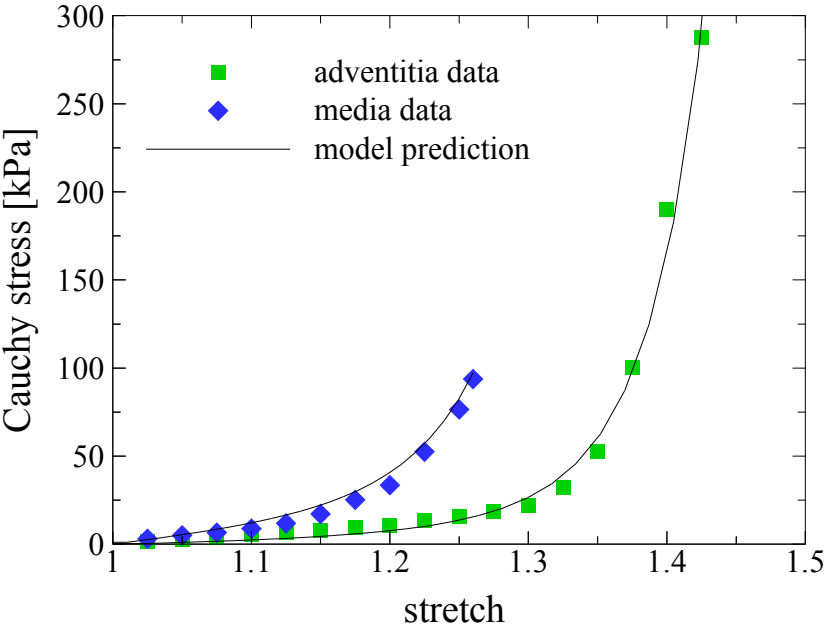


Loads and Boundary Conditions

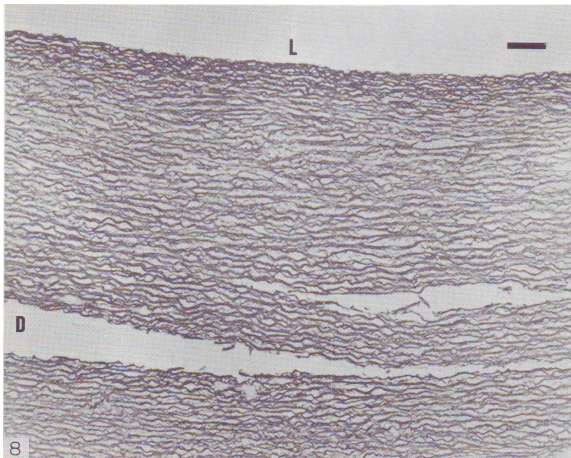
- Axial displacement imposed to provide the physiological *in situ* pre-stretch for healthy arteries, assumed to be $\lambda = 1.2$ [Schulze et al., 2003]. Highly stenotic arteries show very little or no axial *in situ* pre-stretch [Gasser et al. [2007].
- External confinement offered by the surrounding tissues imposed through linear elastic spring elements all around the model (stiffness derived from available literature data [Veress et al. 2002]).
- Growing internal blood pressure:
 - 100 – 110 mmHg (physiological level);
 - 100 – 250 mmHg (overpressure);
- Disregarded in the present calculations:
 - recovering of the unloaded configuration (although already implemented in the finite element code);
 - presence of circumferential residual stresses (experimentally observed).

	K (kPa)	μ (kPa)	k_1 (kPa)	k_2 (-)	γ ($^\circ$)
Adventitia	1667	3.97	37.71	35.74	49
Media	1667	10.77	4.83	4.71	7
Intima-nos	1667	4.91	2.18	2.81	5
Intima-fc	1667	4.59	25.22	10.14	0

Circumferential stress – stretch curves



	Cohesive strength ^a			Fracture energy ^b
	σ_{c1} (kPa)	σ_{c2} (kPa)	σ_{c3} (kPa)	G_c (kJm ⁻²)
A – A	1031.6	951.8	62	1.4
M – M	202.0	188.8	62	1.4
I-nos – I-nos	488.6	943.7	62	1.4
I-fm – I-fm	776.8	277.5	62	1.4
I-fc – I-fc	254.8	468.6	62	1.4



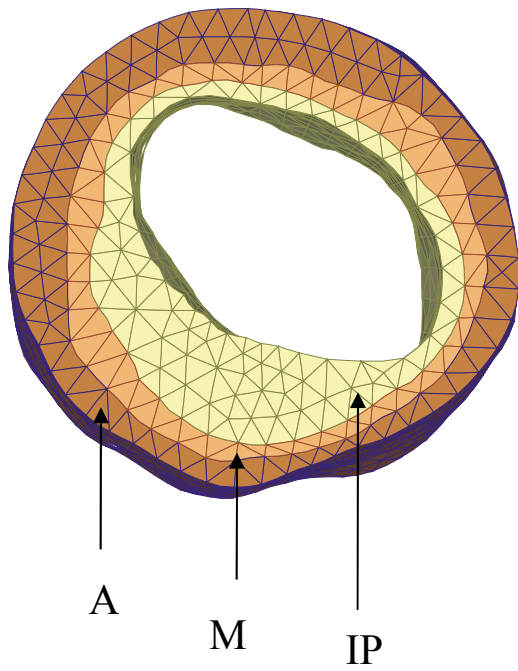
[Carson *et al.*, 1990]

^a σ_{c1} and σ_{c2} from Holzapfel *et al.* 2004.
 σ_{c3} from MacLean *et al.* 1983.

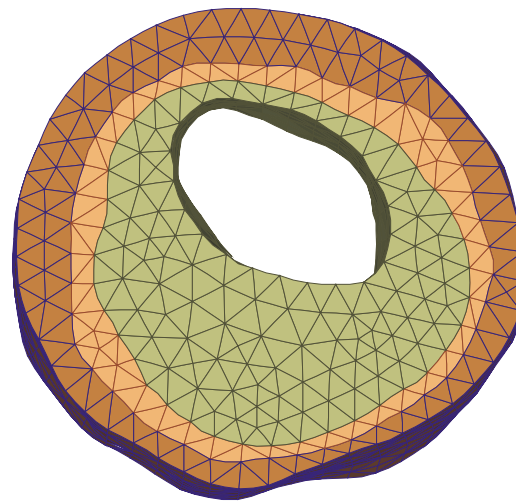
^b G_c from Purslow 1999.

- The geometric variables of the plaque include the degree of stenosis (i.e. the percentage of occlusion) and the presence of lipid pool.

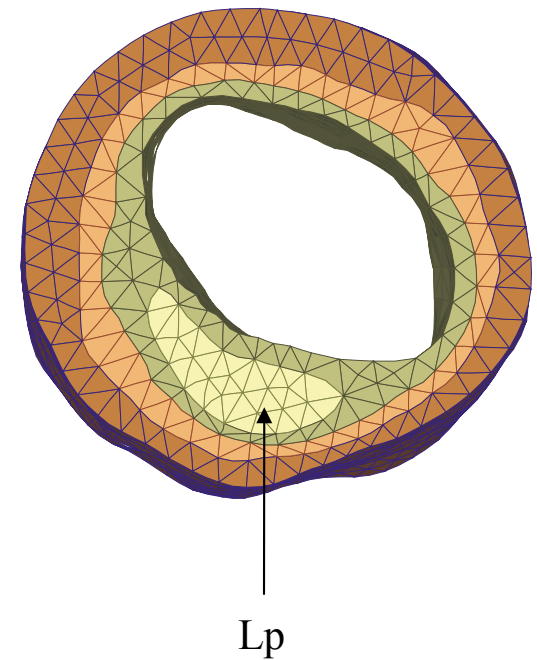
Model 1 – 40% stenosis
(baseline)



Model 2 – 80% stenosis

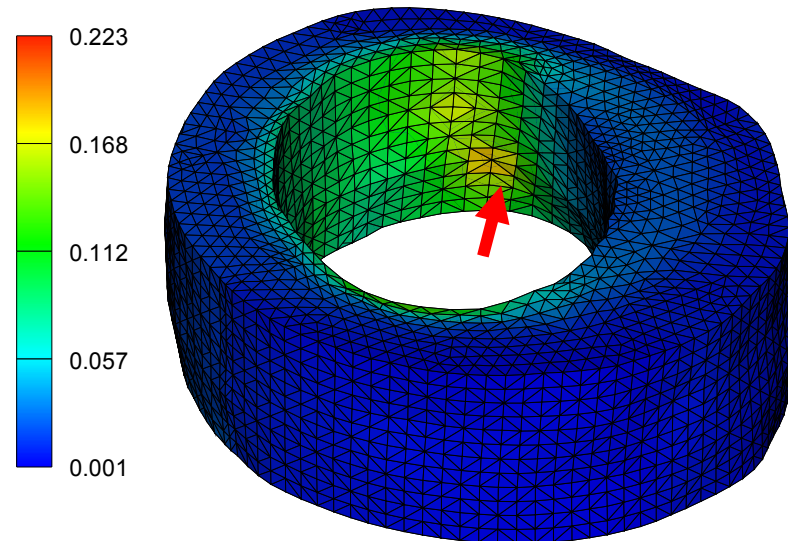


Model 3 – lipid pool
(35% plaque area)



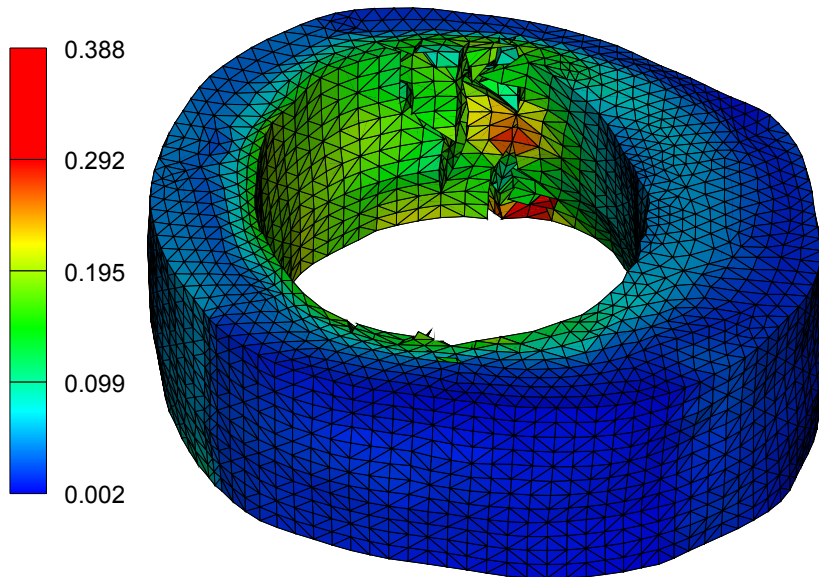
Peak Stress and Intraluminal Pressure

- Plaque rupture is associated with stress in excess of 300 kPa [*Cheng et al., 1993*].
- The peak stress is often used as predictor of plaque rupture
- At 100 mmHg (physiological level) the stress distribution is rather uniform. The luminal pressure is increased up to the formation of the first crack.
- Results in terms of von Mises stress maps.

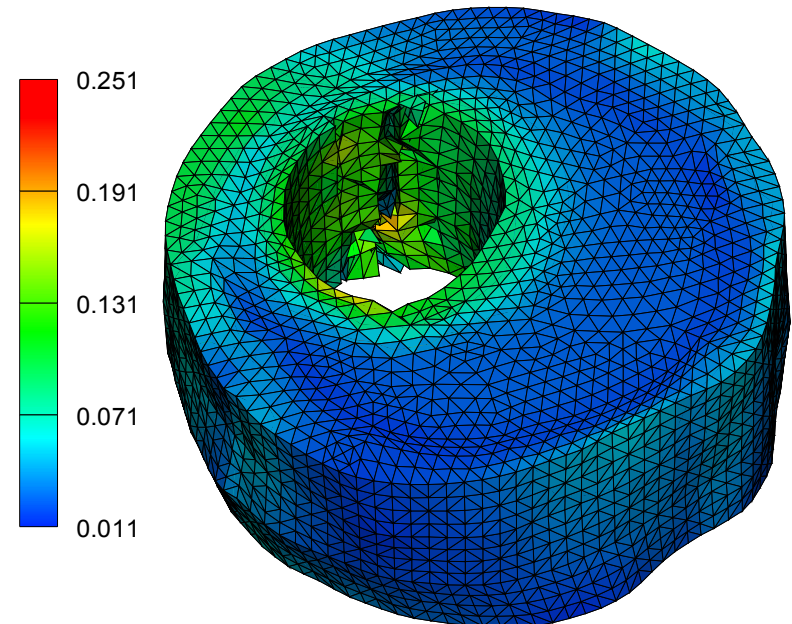


	Pressure (mmHg)	Peak stress (kPa)	σ_{max}/P
Model 1	114	223	14.7
Model 2	263	215	6.1
Model 3	110	303	20.4

- According to *in vitro* testing [*Lendon et al., 1991*] and structural analysis [*Cheng et al., 1993*], plaque rupture occurs at the shoulders. Overpressure crushes the plaque by radial tears exposing the media to the lumen. In the calculations interlayer dissection was not modeled for paucity of experimental data.

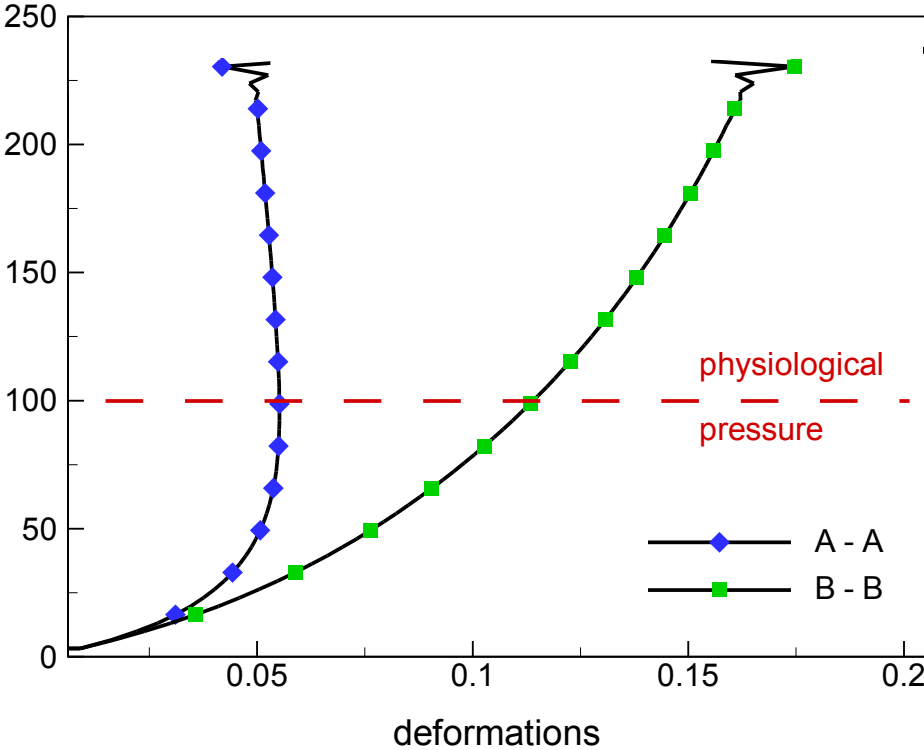
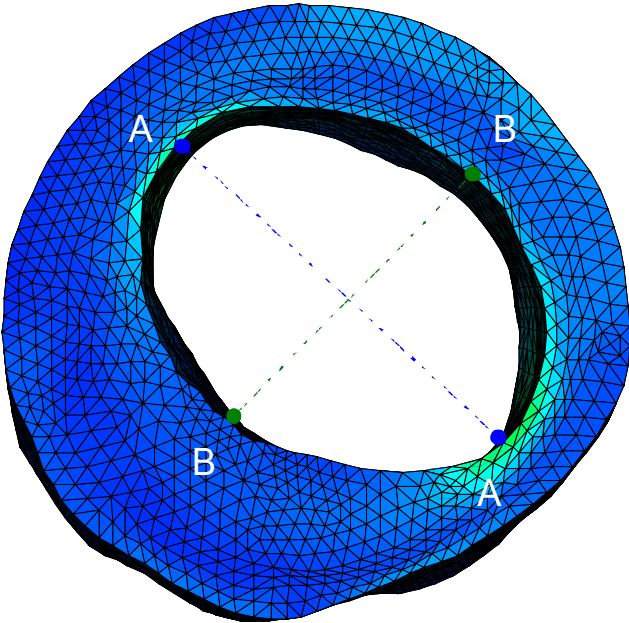


Intraluminal pressure 210 mmHg



Intraluminal pressure 380 mmHg

- Time history of the deformations along the two main directions of the elliptic lumen: A-A and B-B. Upon fracture, the mechanical integrity of the vessel is broken, as shown by the oscillations of the deformation measures.



Conclusions

- Our aim to contribute to a **diagnostic tool** based on numerical simulations of stress distribution and fracture propagation combined with magnetic resonance or ultrasound imaging can be .
- The results obtained during this research represent a first step towards the development of a patient-specific computer tool that may help surgeons in the prediction of the mechanical evolution of atherosclerotic lesions.

LIMITATION: an MRI scan describes the shape of an artery, not its mechanical properties. These parameters vary from patient to patient, depending on the extent of arterial disease.
The key thing is to get more experimental data on human tissue.

- Histology of the arterial wall
- Atherosclerosis
 - histology of the atherosclerotic plaque
 - atherogenesis
- Experimental evidence
- Constitutive material models
 - *orthotropic hyperelastic model* for the arterial wall
 - *transversally isotropic hyperelastic model* for the plaque core
- Cohesive material models
 - *orthotropic model* as generalization of Ortiz and Pandolfi's model [1999]
- Geometrical model
- Numerical simulations
 - stress distribution in atherosclerotic lesions at physiological pressure
 - propagation of fracture during overexpansion

Bibliography

- R. Virmani, F.D. Kolodgie, A.P. Burke, A. Farb, and S.M. Schwartz, 2000. *Lessons from sudden coronary death: a comprehensive morphological classification scheme for atherosclerotic lesions*. Arteriosclerosis, thrombosis, and vascular biology, **20**:1262–1275 .
- G. A. Holzapfel and G. Sommer, 2004. *Anisotropic mechanical properties of tissue components in human atherosclerotic plaques*. Journal of Biomechanical Engineering, **126**:657 – 665.
- H. M. Loree, R. D. Kamm, Stringfellow R. G., and R. T. Lee, 1992. *Effects of fibrous cap thickness on peak circumferential stress in model atherosclerotic vessels*. Circulation Research, **71**:850 – 858.
- P. D. Richardson, M.J. Davis, and G.V.R. Born, 1989. *Influence of plaque configuration and stress distribution on fissuring of coronary atherosclerosis plaque*. Lancet, **2**:941 – 944.
- G.C. Cheng, H.M. Loree and R.D. Kamm and M.C. Fishbein and R.T. Lee, 1993. *Distribution of circumferential stress in ruptured and stable atherosclerotic lesions. A structural analysis with histopathological correlation*. Circulation, **87**: 1179 –1187.
- C.L. Lendon, M.J. Davies and G.V.R .Born. and P.D. Richardson, 1991. *Atherosclerotic plaque caps are locally weakened when macrophages density is increased*. Atherosclerosis, **87**: 87–90.
- N. V. Salunke and L. D. T. Topoleski, 1997. *Biomechanics of atherosclerotic plaque*. Critical Reviews in Biomedical Engineering, **25**:243 – 285.
- M. Ortiz and A. Pandolfi, 1999. *Finitedeformation irreversible cohesive elements for three-dimensional crack-propagation analysis*. International Journal for Numerical Methods in Engineering with Computers, **44**: 1267–1282.